Dalton Transactions

Accepted Manuscript

ROYAL SOCIETY OF CHEMISTRY

www.rsc.org/dalton

Journal Name

ARTICLE

Fabrication of nanocomposites composed of silver cyanamide and titania for improved photocatalytic hydrogen generation

Received 00th January 20xx,
Accepted 00th January 20xx

DOI: 10.1039/x0xx00000x

www.rsc.org/

Hao Meng[a], Xiaoxue Li[a], Xia Zhang†[a], Yufeng Liu‡[b], Yan Xu[a], Yide Han[a] and Junli Xu[a]

The highly efficient composite photocatalysts composed of silver cyanamide (Ag_2NCN) and anatase titania (TiO_2) were fabricated through a chemical precipitation process of silver nitrate and cyanamide in TiO_2 suspensions. The TiO_2 nanoparticles around 15 nm were immobilized on the surface of rectangle Ag_2NCN particles to form hetero-structure, and the contents of TiO_2 were varied to tune the structure and the photocatalytic performances. In comparison with single TiO_2 or Ag_2NCN, the TiO_2/Ag_2NCN nanocomposites exhibited prominent improved photocatalytic activity in the hydrogen generation, and the hydrogen evolution rate (1494.0 μ mol/(g·h)) was higher than most of reported TiO_2-composite photocatalysts. Based on the structure investigation, the photocatalytic mechanism of these TiO_2/Ag_2NCN nanocomposites was proposed. The enhanced photocatalytic activity was attributed to three points: the matched energy level between TiO_2 and Ag_2NCN promoted the electron-hole transfer and thus inhibited the recombination of photo generated electrons and holes; the great electron storage capacity of metallic silver produced in the photocatalytic process also facilitated the charge separation; in addition, the expanded spectrum absorption range because of the composite structure enhanced UV and visible light response ability. These TiO_2/Ag_2NCN nanocomposites also presented good photocatalytic stability in the typical cycle tests. This work provided new insights into fabricating highly efficient composite photocatalysts containing silver and TiO_2 for hydrogen generation.

Introduction

Since the electrochemical decomposition of water at a TiO_2 electrode being reported by Fujishima, the photocatalytic technology has attracted intense attention because of its prospect applications in the environmental purification and renewable energy production.[1, 2] The hydrogen generation through photocatalytic water splitting using solar radiation is regarded as a competitive method due to its green and renewable nature. For carrying out this reaction, the suitable band structure and oxidation-reduction potentials are essential for a good photocatalyst. Specifically, the band gap of the photocatalyst must exceed the theoretical decomposition voltage of H_2O (1.23 V); if taking the over potential into account, the value is needed to reach 1.8 V. In addition, a proper potential position of conduction band is also necessary, which must be more negative than the redox potential of H^+/H_2 (0 V) and H_2O/H_2 (-0.42 V).[3, 4] Moreover, a good response to sunlight and high quantum conversion efficiency are also regarded as important factors in the design of photocatalysts. Recently, considerable efforts have been paid to develop novel photocatalysts in order to achieving higher efficiency for the hydrogen production.[3-5]

TiO_2 is a most widely investigated photocatalyst in the mineralization of organic pollutants as well as hydrogen generation because of its chemical stability, long-term thermodynamic stability, low cost, long-toxicity.[5, 6] However, the wide band gap of TiO_2 (3.2 eV) restricts its activation in ultraviolet irradiation (5% of the total solar spectrum) and thus limits its practical applications. Besides, the easy recombination of photo generated electrons and holes also leads to low photocatalytic efficiency.[6.7] In order to overcome these shortcomings, more and more attentions have been paid to extend its absorption range to visible light and promote photocatalytic efficiency via various surface modification methods. Among these, coupling TiO_2 with another semiconductor with narrow band gap and suitable band potential is proved to be an efficient method. For example, various nanocomposites, such as TiO_2/CdS,[8] TiO_2/PdO,[9] TiO_2/CuO,[10] TiO_2/SnO_x,[11] TiO_2/WO_3,[12] TiO_2/graphene,[6, 13-15] TiO_2/noble metal (Ag, Au, or Pt) ,[16-18] TiO_2-AgX [19, 20] etc, have been reported with improved photocatalytic activity under visible light irradiation.

The metal cyanamide chemistry including its synthetic method and crystallographic study has been enormously progressed over the past decades.[21-33] Especially, in the

[a] Department of Chemistry, College of Sciences, Northeastern University, Shenyang 110819, China
[b] College of Pharmacy, Liaoning University, Shenyang, 110036, China.
† E-mail: xzhang@mail.neu.edu.cn Tel: + 862483684533. Fax: +862483684533.
‡ E-mail: liuyufeng790929@gmail.com

coordination chemistry, the cyanamide anion (NCN^{2-}) serves as a multifunctional coupler in assembling transition-metal units and providing unique properties due to its soft, sterically small, and potentially polydentate nature. As-formed bridged complex is found to have novel structure and special photoconductivity.[21-29] More interestingly, the $[NCN]^{2-}$ ions can adopt two electron forms: the symmetric carbodiimide $[N=C=N]^{2-}$ form [30, 31] and the asymmetrical cyanamide $[N\equiv C-N]^{2-}$ form,[25-29] and both the electron resonance can be found in H_2NCN and some transition-metal cyanamide, such as HgNCN and Ag_2NCN as isomers. The asymmetric form of the $[NCN]^{2-}$ may endow localized dipoles and dipolar fields, which are beneficial to the long-range migration of oppositely charges carried on photocatalysis.[32, 33] Moreover, the delocalized electronic state of $[NCN]^{2-}$ at the valence band maximum (VBM) and the conduction band minimum (CBM) is rather similar to the chalcogenide semiconductors, which implies the potential visible-light photocatalytic property of metal cyanamide. Huang et al [32] firstly reported the photocatalytic activity of $Ag_2[NCN]$. They prepared Ag_2NCN nanoparticles, microparticles and thin films, and investigated their optical, photoelectrochemical properties and photocatalytic activity in the degradation of Methylene blue. More reports about the photocatalytic property of metal cyanamide have not been found to the best of our knowledge.

In this paper, we presented a facile synthetic approach to prepare TiO_2/Ag_2NCN nanocomposites with controlled mass percent of TiO_2. The structure and absorption spectra of these nanocomposites were characterized. The matched energy level between TiO_2 and Ag_2NCN determined an efficient separation of photo generated charges, as a result, the TiO_2/Ag_2NCN nanocomposites exhibited prominent photocatalytic activity in the hydrogen generation from water under simulated sunlight irradiation.

Experimental section

Chemicals

Cyanamide aqueous solution (50 wt%) was purchased from Aladdin Co (China). Silver nitrate, tetrabutyl titanate (TBOT) were supplied by Tianjin Guangfu Fine Chemical Research Institute (China). All the chemicals were of analytic grade and used without further purification, and 18 MΩ/cm deionized water was used throughout the experiments.

Preparation of TiO_2/Ag_2NCN composite photocatalysts

Firstly, TiO_2 nanoparticles were synthesized through a low-temperature hydrothermal method according to our previous work [34]. In a typical synthesis, 20 mL TBOT was dissolved in 200 mL anhydrous ethanol, then, which was quickly mixed with 200 mL deionized water preheated to 70 ° C with pH 3.0 adjusted by 1 M HNO_3. The as-prepared white suspension was maintained at 70 ° C for 48 h. The resulted white precipitate was centrifuged, washed thoroughly with distilled water and dried at 80 ° C for 24 h.

TiO_2/Ag_2NCN nanocomposites were prepared through a facile chemical precipitation process. 125 mL $NH_3\cdot H_2O$ (1.5 M) was added into 20 mL $AgNO_3$ (0.25 M) to get transparent solution, in which a certain amount of TiO_2 nanoparticles were dispersed under vigorous stirring. After that, 5 mL H_2NCN (1 M) solution was added into above suspension and kept stirring for 0.5 h. Finally, the yellow precipitate was centrifuged, washed thoroughly with distilled water, and dried at 60 ° C under vacuum condition. The addition amounts of TiO_2 nanoparticles were 30, 40, 50, 70, 80, 90 and 95 wt% respectively, and as-prepared nanocomposites were labeled as Ti-*x*/ Ag_2NCN, in which the *x* value indicated the TiO_2 addition amount. The pure Ag_2NCN particles were also prepared under same conditions but without TiO_2 addition.

Characterizations

The morphology was observed on a SSX-50 scanning electron microscope (SEM, Shimadzu, Japan). TEM images were obtained by a TECNAIG 220 transmission electron microscope (FEI, USA). X-ray diffraction pattern was taken with a Rigaku XRD D/max-2500PC instrument (CuKα, tube voltage of 50 KV and tube current of 100 mA). FT-IR spectra were recorded using a VERTEX 70 Fourier transform infrared spectrophotometer (Bruker, Germany), and the samples were dispersed in anhydrous KBr. The UV-Vis diffuse reflectance spectra were measured using a Perkin Elmer Lamdba 35 UV-Vis spectrophotometer, and the wavelength was ranged from 200 to 800 nm. Photoluminescence (PL) spectra were measured using a Fluoromax-4 photoluminescence spectrophotometer (HORIBA Scientific, France) under 320 nm excitation and the slit widths at the excitation and emission of the spectrofluorimeter were 5 and 2 nm, respectively. X-ray photoelectron spectra (XPS) was conducted on an ESCALAB 250Xi (Thermo Fisher Co., USA) using an Al-Kα monochromatic x-ray (1486.6 eV) as source.

Photocatalytic hydrogen generation

Photocatalytic hydrogen production reaction was carried out in a closed gas-circulating system. 200 mg catalysts were suspended in a mixture of 100 mL deionized water and 10 mL methanol as hole scavenger. The obtained homogeneous suspensions were filled in a glass reactor with top quartz window and a water cooling jacket. The reaction cell was degassed for 10 min by a vacuum bump and then was irradiated under a 300 W Xenon lamp. The distance between the reaction bottle and light source was maintained at 10 cm, and the light irradiation density was 94.30 mw/cm^2. The hydrogen evolution was measured every 1 h with an online gas chromatograph (GC7900, TECHCOMP Ltd. Co., China) equipped with a TCD detector. After the photocatalysis, the suspension was centrifuged and dried to regain the photocatalysts for the post-catalytic characterization or typical cycle experiments.

Results and discussion

Characterization of TiO_2/Ag_2NCN composite particles

The morphologies of pure Ag_2NCN, TiO_2 and TiO_2/Ag_2NCN nanocomposites were shown in Fig.1. As shown in Fig. 1(a), the single Ag_2NCN was rectangle particles with smooth surface, which size was around 600-700 nm in length and 200-400 nm in width. After TiO_2 addition, as shown in Fig. 1 (b)-(f), the morphology of Ag_2NCN particles remained rectangle and the size of that had not changed. However, the surface of these rectangle particles became

very rough, and some small particles were clearly observed. It suggested that TiO_2 nanoparticles were immobilized on the surface

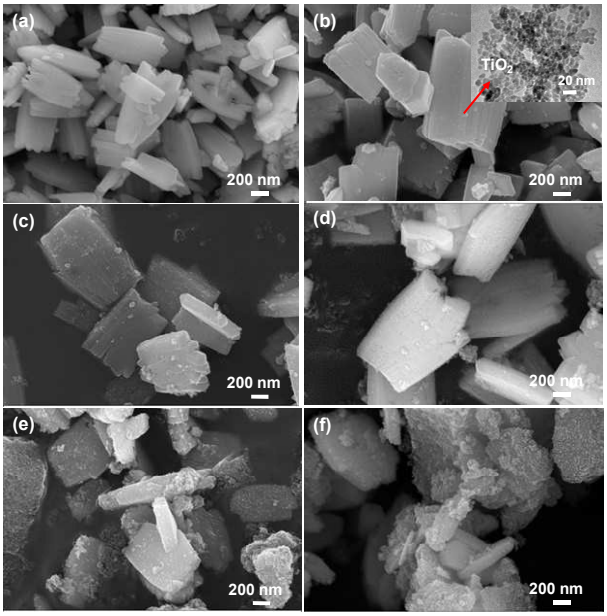

Fig. 1 SEM images of Ag_2NCN (a) and TiO_2/Ag_2NCN composite particles with different TiO_2 additions. (b)30 wt%; (c) 40 wt%; (d) 50 wt%; (e) 80 wt%; (f) 90 wt%. The top insert in Fig.(b) is the TEM image of pure TiO_2 nanoparticles

of Ag_2NCN and fabricated composite structure. The detailed investigation of these TiO_2 nanoparticles could be observed from the top inset in Fig. 1 (b), the size of which was about 15 nm. As the TiO_2 addition was ranged from 30 to 50% (Fig.1(b)-(d)), the TiO_2 nanoparticles were relatively dispersed on the surface of Ag_2NCN. And with the TiO_2 addition increasing to 80 and 90%, as shown in Fig. 1(e) and (f), more TiO_2 nanoparticles were found to be agglomerated.

Powder XRD patterns of these TiO_2/Ag_2NCN composite particles were presented in Fig. 2(a). In the case of the composite particles except Ti-90/Ag_2NCN, the main diffraction was attributed to anatase TiO_2 (JCPDS no. 21-1272) and monoclinic Ag_2NCN (JCPDS no. 70-523). Besides, a weak diffraction at $2\theta = 44.3^{O}$ could be assigned to cubic Ag (JCPDS no. 04-0783), which implied that a bit of metallic Ag was existed on the surface of TiO_2/Ag_2NCN composite particles. For the sample of Ti-90/Ag_2NCN, apart from the characteristic diffraction peaks of anatase TiO_2, the peaks corresponding to Ag_2NCN became weak, that could be understood as the diminished content of Ag_2NCN. According to Scherrer's equation:

$$D = \frac{K\lambda}{\beta \cos\theta}$$

(K=0.89, λ=0.154056 nm), based on the data of (101) plane ($2\theta = 25.2^{O}$) of anatase TiO_2, the average crystalline size of TiO_2 particles was about 6 nm.

The FT-IR spectra of pure Ag_2NCN and Ti-50/Ag_2NCN nanocomposites were measured and shown in Fig. 2(b). The characteristic IR absorption of $[NCN]^{2-}$ was found in both IR spectra.[21, 35] For example, the peaks at 1980 and 1280 cm^{-1} were assigned to the asymmetric stretching frequency and symmetric stretching mode; the peaks at 1190 and 630 cm^{-1} were ascribed to the deformation vibration of $[NCN]^{2-}$. For the TiO_2/Ag_2NCN

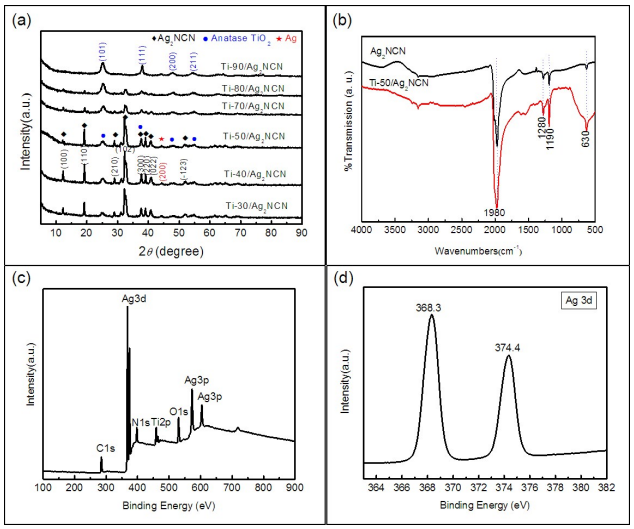

Fig.2 (a) XRD patterns of TiO_2/Ag_2NCN composite particles; (b)FT-IR spectra of Ag_2NCN and Ti-30/Ag_2NCN nanocomposites; (c) Broad XPS spectrum of Ti-50/Ag_2NCN nanocomposites; (d) Ag3d XPS spectrum of Ti-50/Ag_2NCN nanocomposites

nanocomposites, apart from above characteristic peaks of $[NCN]^{2-}$, a broad peak ranging from 860 to 500 cm^{-1} could be attributed to the stretching vibration mode of Ti-O.[16] The FT-IR results indicated that there was no chemical bond between TiO_2 and Ag_2NCN particles.

XPS spectrum of Ti-50/Ag_2NCN nanocomposites was also measured to clarify the element composition and the chemical state of elements. As shown in Fig. 2 (c), the full-scale XPS pattern indicated the existence of Ag, C, Ti, N and O, and the binding energies of Ag 3d, Ti 2P, C 1s, N 1s and O 1s were 368.3, 458.8, 286.0, 398.3 and 529.3 eV respectively. A high-resolution XPS spectrum of Ag 3d (Fig. 2 d) presented the binding energies of Ag $3d_{5/2}$ and Ag $3d_{3/2}$ was 368.3 and 374.4 eV, respectively. It was reported [6, 36,37] that the 3d peaks of metallic Ag were centered at 367.9 and 373.9 eV, while which for the Ag (I) exhibited at 369.4 and 375.6 eV. Therefore, it was suggested that small amount of metallic Ag existed on the surface of Ti-50/Ag_2NCN, which was probably caused by the slightly photo-induced reduction of Ag(I) in the synthesis of composite particles. The above XPS analyses were consistent with the XRD results.

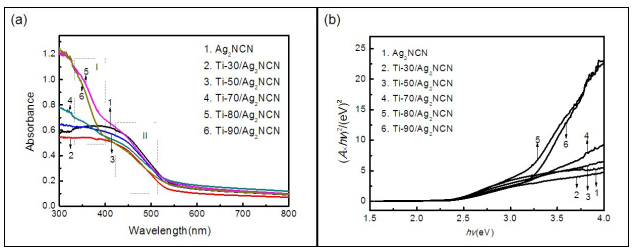

Fig. 3 (a) UV-Vis diffuse reflectance spectra of Ag_2NCN and TiO_2/Ag_2NCN composite particles; (b) The plot curves of $(A\times h\nu)^2$ vs($h\nu$) of Ag_2NCN and TiO_2/Ag_2NCN nanocomposites

Fig. 3(a) showed the UV-Vis diffuse reflectance spectra of these Ag_2NCN and TiO_2/Ag_2NCN composite particles. As shown in Fig. 3(a), pure Ag_2NCN exhibited strong absorption in the visible region. In the case of TiO_2/Ag_2NCN composite particles, two absorption edges were observed. One was attributed to the band gap transition of TiO_2 (area I in the UV region) and the other was of Ag_2NCN (area II in the visible region). The UV-Vis spectra implied that as-prepared TiO_2/Ag_2NCN composite particles have excellent absorption capacity in both UV and visible region.

Based on the formula: $A=\frac{C(h\nu-E_g)^{1/2}}{h\nu}$ a plot of the calculated $(A\times h\nu)^2$ as a function of light energy ($h\nu$) was shown in Fig. 3(b). The extrapolation of the linear regions in the plots suggested the associated direct band gap was 2.34, 2.25, 2.18, 2.13, 2.06 and 2.01 eV corresponding to Ag_2NCN and Ti-*x*/Ag_2NCN, while the *x* values were 30, 50, 70, 80 and 90 respectively. The above results indicated a red shift in the absorption edge of nanocomposites as compared with pure Ag_2NCN.

PL quenching effect is usually applied to explore the charge transfer efficiency within composite materials, which is an important factor affected the photocatalytic efficiency. The PL spectra of TiO_2/Ag_2NCN nanocomposites with various TiO_2 contents were shown in Fig. 4. It was observed that the PL intensity of TiO_2/Ag_2NCN nanocomposites was evidently lower than that of TiO_2, which suggested an efficient electron transfer between TiO_2 and Ag_2NCN. The above PL results determined an enhanced photocatalytic property for TiO_2/Ag_2NCN nanocomposites.

Photocatalytic hydrogen generation

The photocatalytic hydrogen generation activities of TiO_2, Ag_2NCN and TiO_2/Ag_2NCN nanocomposites under simulated sunlight irradiation were tested and shown in Fig. 5. It could be seen that the pure Ag_2NCN had no photocatalytic activity, which might be due to the rapid recombination of photogenerated electrons and holes. For the pure TiO_2, Ti-30/Ag_2NCN and Ti-40/Ag_2NCN, a small amount of hydrogen were produced. When the TiO_2 addition increased from 50% to 90%, a significant improved hydrogen generation

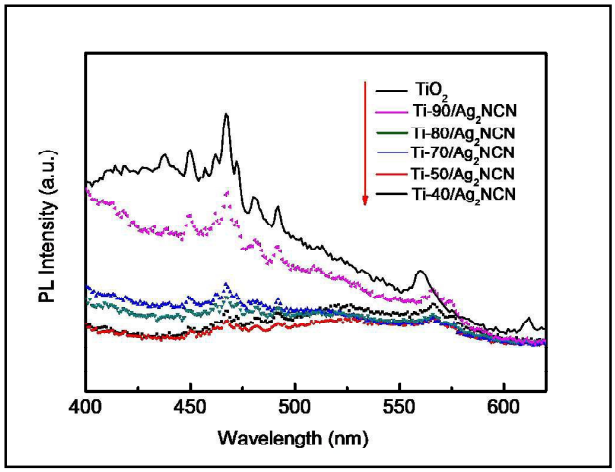

Fig. 4 Photoluminescence spectra of TiO_2 and TiO_2/Ag_2NCN composite particles

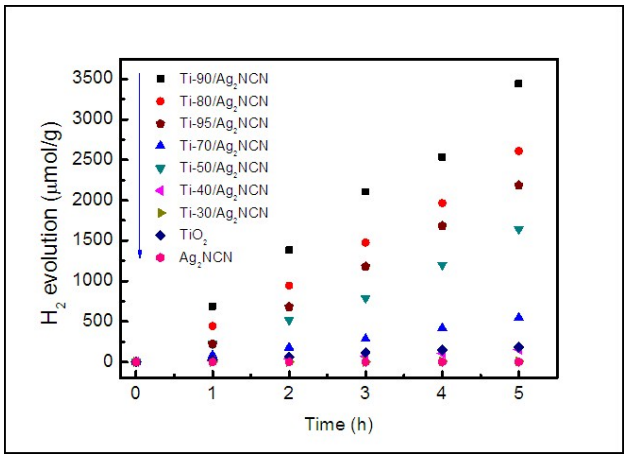

Fig. 5 Photocatalytic hydrogen generation capacity by TiO_2 and TiO_2/Ag_2NCN nanocomposites as a function of irradiation time

capacity could be observed. However, continually increasing the TiO_2 addition to 95%, a reduced hydrogen generation capacity within 5 h was observed. The hydrogen production capacities within 5 h were 3440.2, 2606.6, 2186.6,1642.0 and 546.6 μ mol/g while the TiO_2 addition was 90, 80, 95, 50 and 70% accordingly. Obviously, the fabrication of composite structure with a determined composition of both semiconductors had a positive influence on the photocatalytic activity. In this work, the TiO_2/Ag_2NCN nanocomposites with 90 wt% TiO_2 and 10 wt % Ag_2NCN presented the best photocatalytic activity in the hydrogen generation.

For a composite photocatalyst, the uniformity of the composite structure and the close contact between two components are favor for the separation of photo generated electron -hole pairs and thus promote the photocatalytic efficiency. [45] In the case of the as-prepared composite samples, the uniformity of TiO_2 nanoparticles and more close contact interface between TiO_2 and Ag_2NCN are both important in improving the photocatalytic efficiency. Considering the different size of TiO_2 and Ag_2NCN, which for TiO_2 was about 15 nm and for Ag_2NCN was 600-700 nm in length and 200-400 nm in width, in order to achieve more close contact interface, it must be more TiO_2 nanoparticles deposited on the Ag_2NCN. In our experiments, the sample Ti-90/Ag_2NCN with the molar ratio of TiO_2 and Ag_2NCN of 28.8:1 presented best photocatalytic activity. Continuously increasing the mol number of TiO_2 (Ti-95/Ag_2NCN), the photocatalytic activity but decreased, that might be caused by the reduced uniformity of TiO_2. The similar results were obtained by other TiO_2-composites, such as TiO_2-graphene nanoplatelets with 97 wt% TiO_2 and 3 wt% graphene [7] and TiO_2-Bi_2WO_6 with the mol ration of TiO_2 and Bi_2WO_6 was 6:1 presented higher photocatalytic activity. [46]

To further study the photocatalytic stability of these TiO_2/Ag_2NCN nanocomposites, a typical time-course hydrogen generation tests over the Ti-90/Ag_2NCN and Ti-50/Ag_2NCN catalysts were conducted for 50 h with the evacuation every 5 h, and the results were shown in Fig. 6. Interestingly, both TiO_2/Ag_2NCN nanocomposites present continuous increased photocatalytic

activities at first several cycles, and reached their maximum hydrogen production capacity and then decreased slightly. For the Ti-90/Ag_2NCN nanocomposites, their maximum hydrogen production capacity appeared at fifth cycle with a hydrogen evolution of 7469.8 μmol/g, and after 10 cycles, the hydrogen evolution was kept at 4208.7 μmol/g, which value was higher than the result of the first cycle. For Ti-50/Ag_2NCN nanocomposites, their maximum hydrogen production was obtained at seventh cycle, and after 10 cycles, the hydrogen evolution was 3202.0 μmol/g, which was also higher than the data at first cycle.

According to above results, the maximum hydrogen generation rate of Ti-90/Ag_2NCN nanocomposites could reach 1494.0 μmol/(g·h). For comparison, some reported hydrogen evolution rate by TiO_2-composites was listed in Table 1. From Table 1, it could be concluded that the as-prepared nanocomposites had good photocatalytic hydrogen generation efficiency under simulated sunlight irradiation. In addition, as presented in our previous work,[42] these TiO_2/Ag_2NCN nanocomposites also possessed good activity in the photocatalytic degradation of organic dyes.

Discussion on photocatalytic mechanism

The cycle tests revealed that the TiO_2/Ag_2NCN nanocomposites showed an enhanced photocatalytic activity at first several cycles, and after 10 cycles, which still have a higher photocatalytic hydrogen generation ability. To explore the photocatalytic process, the morphology and structure of the TiO_2/Ag_2NCN nanocomposites after the photocatalytic tests were investigated.

The PXRD patterns of the TiO_2/Ag_2NCN nanocomposites collected after photocatalytic tests were measured to determine their structure stability in the photocatalysis. As shown in Fig. 7(a), an obvious difference from the patterns shown in Fig. 2(a) was that the peak intensity of metallic Ag located at 2θ = 44.3, 64.4 and 77.3 ^{O} enhanced. A more detailed comparison of XRD patterns of Ti-50/Ag_2NCN nanocomposites before and after photocatalytic experiments was presented in Fig. 7(b). It could be seen clearly that the diffraction assigned to Ag_2NCN became weak, while the characteristic diffraction of anatase TiO_2 and metallic Ag enhanced. The PXRD results indicated that more metallic Ag were produced in the photocatalysis, which might participated in the photocatalytic hydrogen generation.

XPS survey spectrum and high-resolution XPS spectrum of Ag 3d of Ti-50/Ag_2NCN sample after photocatalysis were also measured to determine the effect of photocatalysis on the elements composition.

Table 1 Comparison of H_2 evolution rate from literature

Composites	H_2 evolution (μmol/(g·h))	Incident light	Ref.
Ag/RGO*/TiO_2	196.87	Xe lamp(500 W)	[6]
TiO_2-Ag	892	Hg-Xe arc lamp (240 W)	[16]
TiO_2-RGO	740	Xe lamp(200 W)	[38]
TiO_2-RGO	500	UV-visible light (150mW/cm^2)	[39]
TiO_2-CuO	1100	Xe lamp(500 W)	[40]
TiO_2-MoS_2-graphene	2066	Xe lamp (350 W)	[41]
Pt-TiO_2-C	53	Xe lamp (300 W)	[47]
Sn_3O_4-TiO_2	83.5	Xe lamp (300 W)	[48]
Au-TiO_2-CdS	1970	Xe lamp (300 W)	[49]

* RGO- reduced graphene oxide

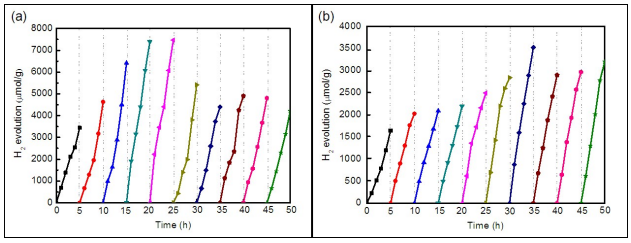

Fig. 6 A typical time course of hydrogen production over Ti-90/Ag_2NCN (a) and Ti-50/Ag_2NCN (b) nanocomposites, five runs is one continuous reaction.

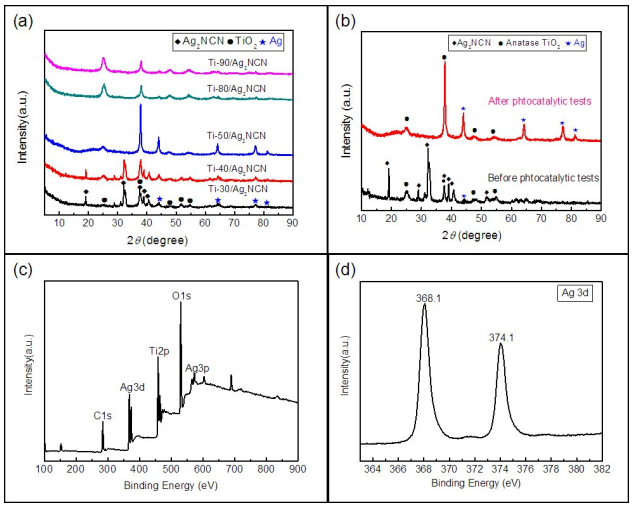

Fig. 7 (a) PXRD patterns of TiO_2/Ag_2NCN composite particles after photocatalytic tests; (b) PXRD patterns comparison of Ti-50/Ag_2NCN before and after photocatalytic tests; (c) Broad XPS spectrum and (d) Ag3d XPS spectrum of of Ti-50/Ag_2NCN nanocomposites after photocatalytic tests.

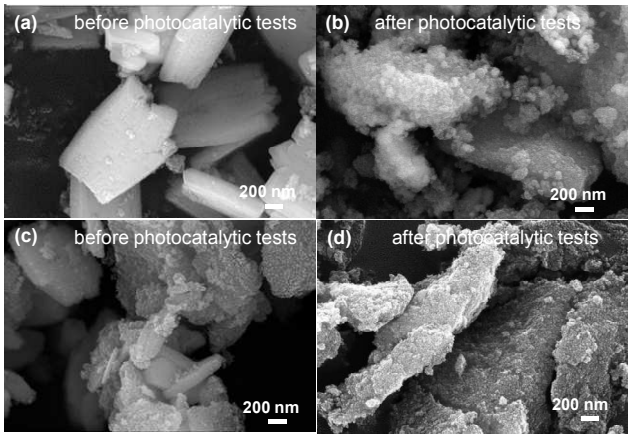

Fig. 8 SEM images of Ti-50/Ag_2NCN (a, b) and Ti-90/Ag_2NCN (c,d) before and after photocatalysis.

As shown in Fig. 7(c), the constituent elements of nanocomposites had no change after photocatalysis. However, the binding energies of the Ag $3d_{5/2}$ and Ag $3d_{3/2}$, as shown in Fig. 7(d), were shifted to 368.1 and 374.1 eV, respectively, which was more close to the data of metallic Ag.[6] The XPS analyses also verified the increased amount of metallic Ag for the TiO_2/Ag_2NCN nanocomposites after photocatalysis.

Fig. 8 showed the morphology investigation before and after photocatalytic experiments for Ti-50/Ag_2NCN and Ti-90/Ag_2NCN. It could be seen that the surface morphology of two samples changed evidently after the photocatalytic tests. The surface of composite particles became rougher, and much more tiny particles were deposited on the top surface of Ag_2NCN, considering the PXRD and XPS results, which might be the metallic Ag produced by the reduction of Ag(I). The EDX spectra of the as-prepared Ti-90/Ag_2NCN before and after photocatalytic tests were shown in Fig. S1. It was observed that the element composition and the weight percent of element Ag was not changed evidently after photocatalytic tests. Though the metallic Ag was produced by the reduction of Ag_2NCN in the photocatalysis, however, the total content of element Ag had not changed, as a result, the intensity of EDX peak of element Ag had not changed after photocatalysis.

Above results determined that more metallic Ag particles were formed on the top surface of nanocomposites in the photocatalytic process. It was reported that metallic Ag or Au nanoparticles are effective additives for metal-TiO_2 composites. The localized surface plasmon effect of Au or Ag promotes the visible-light response of the samples, meanwhile, the fast electron-transfer ability of metallic Au or Ag also effectively restrains the recombination of electron and hole and promotes the quantum conversion efficiency.[6, 43, 44] Therefore, the metallic Ag existed on the top surface of the TiO_2/Ag_2NCN nanocomposites might be the main reason for the improved photocatalytic hydrogen generation efficiency and good photocatalytic stability in the typical cycle experiments.

Furthermore, compared to pure Ag_2NCN and TiO_2 particles, the TiO_2/Ag_2NCN nanocomposites with TiO_2 contents ranging from 50 % to 95 % showed significantly enhanced hydrogen generation activity under xenon lamp irradiation. In order to clarify the photocatalytic mechanism, the Mott-Schottky plot of single Ag_2NCN and TiO_2 was conducted and the potential of conduction band (CB) and valence band (VB) of two semiconductors were determined in our previous work.[42] The potential of CB and VB versus saturated calomel electrode (SCE) were -0.97 V and 1.37 V for Ag_2NCN, while -0.89V and 2.21 V for TiO_2 respectively. Based on that, the photocatalytic hydrogen generation mechanism of as-prepared TiO_2/Ag_2NCN nanocomposites was illustrated in Fig. 9.

According to previous UV-Vis spectra (Fig. 3), both the UV and visible light could be absorbed by TiO_2/Ag_2NCN nanocomposites in generating electrons and holes simultaneously. As shown in Fig. 9, the visible part of the incident light was absorbed by Ag_2NCN, and generated electrons tended to transfer to the CB of TiO_2. At the same time, the UV part of the incident light was absorbed by TiO_2.

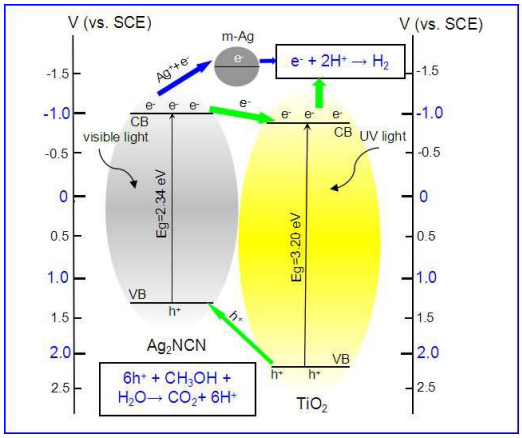

Fig. 9 Sketching map of energy band structure and charge separation of TiO_2/Ag_2NCN composite particles.

and the generated holes tended to transfer to the VB of Ag_2NCN. On the other hand, the metallic Ag produced on the top surface of composite particles also participated in the photocatalysis, which exhibited great electron storage capacity and acted as an electron tank and facilitated charge separation.[6] Because of that, an efficient charge separation was occurred at the interface of TiO_2 and Ag_2NCN, which restrained the recombination of photo-induced electrons and holes and thus promoted the photocatalytic efficiency. Furthermore, the hetero-structure of the TiO_2/Ag_2NCN nanocomposites had more active centers, which provided adequate electrons for the reduction of H^+, that also facilitate the photocatalytic hydrogen generation.

Conclusions

In summary, a novel composite structure of TiO_2/Ag_2NCN with excellent photocatalytic hydrogen generation activity and good photocatalytic stability were synthesized using a facile chemical method. The anatase TiO_2 nanoparticles around 15 nm were deposited on the surface of rectangle Ag_2NCN particles and thus formed hetero-structure. In the photocatalytic hydrogen generation, the as-prepared TiO_2/Ag_2NCN nanocomposites

exhibited enhanced photocatalytic activity in comparison with pure TiO_2 and Ag_2NCN, and the maximum H_2 evolution reached 7469.8 μ mol/g in 5 h, which value was higher than most reported results of TiO_2-containing samples. More importantly, these TiO_2/Ag_2NCN nanocomposites kept good photocatalytic stability in the cycle photocatalysis. The photocatalytic mechanism analyses indicated that the enhanced absorption toward UV and visible light, efficient separation of photo-induced electrons and holes and increased active centers were responsible for the the enhanced photocatalytic activity of TiO_2/Ag_2NCN nanocomposites. This work suggested a promising TiO_2-Ag based system with high photocatalytic performance in the hydrogen production.

Acknowledgements

The authors are very grateful for the financial support of National Natural Science Foundation of China (No. 21501023, 21103017, 51104042).

References

1 A. Fujishima and K. Honda, *Nature*, 1972, **238,** 37-38.
2 S. Y. Dong, J. L. Feng, M. H. Fan, Y. Q. Pi, L. M. Hu, X. Han, M. L. Liu, J. Y. Sun and J. H. Sun, *RSC Adv.*, 2015, **5,** 14610-14630.
3 X. B. Chen, C. Li, M. Grätzel, R. Kostecki and S. S. Mao, *Chem. Soc. Rev.*, 2012, **41,** 7909-7937.
4 Z. W. Zhao, Y. J. Sun and F. Dong, *Nanoscale,* 2015, **7,** 15-37.
5 L. Clarizia, D. Spasiano, I. D. Somma, R. Marotta, R. Andreozzi and D. D. Dionysiou, *Int. J. Hydrogen energy*, 2014, **39,** 16812-16831.
6 W. Y. Gao, M. Q. Wang, C. X. Ran, X. Yao, H. H. Yang, J. Liu, D. He and J. B. Bai, *Nanoscale*, 2014, **6,** 5498-5508.
7 F. N. Sayed, R. Sasikala, O. D. Jayakumar, R. Rao, C. A. Betty, A. Chokkalingam, R.M. Kadam, Jagannath, S. R. Bharadwaj, A. Vinu and A. K. Tyagi, *RSC Adv.*, 2014, **4,** 13469-13476.
8 S. Dutta, R. Sahoo, C. Ray, S. Sarkar, J. Jana, Y. Negishi and T. Pal, *Dalton Trans.*, 2015, **44,** 193-201.
9 S. Choudhury, R. Sasikala, V. Saxena, D. K. Aswal and D. Bhattacharya, *Dalton Trans.*, 2012, **41,** 12090-12095.
10 L. L. Zhu, M. H. Hong and G. W. Ho, *Nano Energy*, 2015, **11,** 28-37.
11 Q. Gu, J. L. Long, H. Q. Zhuang, C. Q. Zhang, Y. G. Zhou and X. X. Wang, *Phys. Chem. Chem. Phys.*, 2014, **16,** 12521-12534.
12 C. W. Lai and S. Sreekantan, *Int. J. Hydrogen Energy*, 2013, **38**(5), 2156-2166.
13 A. P. Bhirud, S. D. Sathaye, R. P. Waichal, J. D. Ambekar, C. J. Park and B.B. Kale, *Nanoscale*, 2015, **7,** 5023-5034.
14 P. K. Dubey, P. Tripathi, R. S. Tiwari, A. S. K. Sinha and O.N. Srivastava, *Int. J. Hydrogen Energy*, 2014, **39,** 16282-16292.
15 F. Y. Pei, Y. L. Liu, L. Zhang, S. P. Wang, S. G. Xu and S. K. Cao, *Mater. Res. Bull.*, 2013, **48**(8), 2824-2831.
16 T. N. Ravishankar, T. Ramakrishnappa, H. Nagabhushana, V. S. Souza, J. Dupont and G. Nagaraju, *New J. Chem.*, 2015, **39,** 1421-1429.
17 L. Zhang, N. Q. Pan and S. W. Lin, *Int. J. Hydrogen Energy*, 2014, **39**(25), 13474-13480.
18 Y. Wang, J. G. Yu, W. Xiao and Q. Li, *J. Mater. Chem. A*, 2014, **2,** 3847-3855.
19 D. W. Wang, Y. Li, G. L. Puma, C. Wang, P. F.Wang, W. L. Zhang and Q. Wang, *Appl. Catal. B*, 2015, 168–169, 25-32.
20 C. G. Liu, Z. F. Lei, Y. N. Yang and Z. Y. Zhang, *Water Res.*, 2013, **47**(14), 4986-4992.
21 X. H. Liu, P. Mu1ller, P. Kroll and R. Dronskowski, *Inorg. Chem.* 2002, **41**(16), 4259-4265.
22 S. M. P. R. M. Cunha, M. F. C. Guedes da Silvaa and A. J. L. Pombeiro, *J. Chem. Soc. Dalton Trans.,* 2002, 1791–1799.
23 L. M. D. R. S. Martíns, E. C. B. A. Alegria, D. L. Jughes, J. J. R. Fraústo da Silva and A. J. L. Pombeiro, *Dalton Trans.*, 2003, 3743-3750.
24 Y. Tanabe, H. Kajitani, M. Iwasaki and Y. Ishii, *Dalton Trans.*, 2007, 4701-4707.
25 X. Liu, A. Decker, D. Schmitz and R. Dronskowski, *Z. Anorg. Allg. Chem.*, 2000, **626,** 103-105.
26 M. Becker and M. Jansen. *Z. Anorg. Allg. Chem.*, 2000, **626,** 1639-1641.
27 W. P. Liao, C. H. Hu, R. K. Kremer and R. Dronskowski., *Inorg. Chem.,* 2004, **43,** 5884-5890.
28 M. Becker, J. Nuss and M. Jansen., *Z. Naturforsch*., 2000, **55b**, 383-385.
29 R. Cao and K. Tatsumi, *Chem. Commun.*, 2002, 2144-2145.
30 X. H. Liu, M. Krott, P. Muller, C. H. Hu, H. Lueken and R. Dronskowski, *Inorg. Chem.,* 2005, **44,** 3001-3003.
31 X. H. Liu, R. Dronskowski, R. K. Kremer, M. Ahrens, C. H. Lee and M. H. Whangbo, *J. Phys. Chem. C*, 2008, **112,** 11013-11017.
32 W. Zhao, Y. F. Liu, J. J. Liu, P. Chen, I. W. Chen, F. Q. Huang and J. H. Lin, *J. Mater. Chem. A,* 2013, **1,** 7942-7948.
33 K. L. Zhang, C. M. Liu, F. Q. Huang, C. Zheng and W. D. Wang, *Appl. Catal. B*, 2006, **68,** 125-129.
34 S. G. Guo, J. H. Zhang, M. S. Shao, X. Zhang, Y. F. Liu, J. L. Xu, H. Meng and Y. D. Han, *Mater. Res. Express*, 2015, **2,** 045101.
35 S. K. Deb and A. D. Yoffe, *Tans. Faraday Soc.* 1959, **55,** 106-113.
36 V. G. Pol, D. N. Srivastava, O. Palchik, V. Palchik, M. A. Slifkin, A. M. Weiss and A. Gedanken, *Langmuir*, 2002, **18,** 3352-3357.
37 X. P. Sun, S. J. Dong and E. K. Wang, *Macromol.*, 2004, **37,** 7105-7108.
38 W. Fan, Q. Lai, Q. Zhang and Y. Wang, *J. Phys. Chem. C*, 2011, **115**, 10694-10701.
39 J. Shen, Y. Long, T. Li, M. Shi, N. Li and M. Ye, *Mater. Chem. Phys.*, 2012, **133,** 480-486.
40 B. W. Wang, Q. M. Sun, S. H. Liu and Y. P. Li, *Int. J. hydrogen energy*, 2013, **38**(18), 7232-7240.
41 Q. Xiang, J. Yu and M. Jaroniec, *J. Am Chem. Soc*, 2012, **134,** 6575-6578.
42 X. Li, X. Zhang, Z. F. Zhu, G. Q. Lin, Y. B. Li, X. X. Li and J. L. Xu, *Chem. J. Chinese U.*, 2015, **36**(2), 361-367.
43 M. S. A. S. Shah, K. Zhang, A. R. Park, K. S. Kim, N. G. Park, J. H. Park and P. J. Yoo, *Nanoscale*, 2013, **5,** 5093-5101.
44 M. Teranishi, S. I. Naya and H. Tada, *J . Am. Chem. Soc.*, 2010, **132,** 7850-7851.
45 J. Zhou, G. H. Tian, Y. J. Chen, J. Q. Wang, X. R. Cao, Y. H. Shi, K. Pan and H. G. Fu, *Dalton Trans.*, 2013, **42,** 11242-11251.

46 Y. F. Hou, S. J. Liu, J. H. Zhang, X. Cheng and Y. Wang, *Dalton Trans.*, 2014, **43,** 1025-1031.
47 M. Kim, A. Razzaq, Y. K. Kim, S. Kim and S. In, *RSC Adv.*, 2014, **4,** 51286–51293.
48 G. H. Chen, S. Z. Ji, Y. H. Sang, S. J. Chang, Y. N. Wang, P. Hao, J. Claverie, H. Liu and G. W. Yu, *Nanoscale*, 2015, **7,** 3117–3125.
49 J. Fang, L. Xu, Z. Y. Zhang, Y. P. Yuan, S. W. Cao, Z. Wang, L. S. Yin, Y. S. Liao and Can Xue, *ACS Appl. Mater. Interfaces*, 2013, **5 (16)**, 8088–8092.

Graphical abstract.